Catalysis Today 175 (2011) 420–429

Contents lists available at ScienceDirect

Catalysis Today

journal homepage: www.elsevier.com/locate/cattod

Catalytic activities of Re–Ni/CeO_2 bimetallic catalysts for water gas shift reaction

Kingkaew Chayakul, Tipaporn Srithanratana, Sunantha Hengrasmee*

Department of Chemistry and Center for Innovation in Chemistry, Faculty of Science, Khon, Kaen University, Khon Kaen 40002, Thailand

ARTICLE INFO

Article history:
Received 11 October 2010
Received in revised form 27 April 2011
Accepted 24 May 2011
Available online 23 June 2011

Keywords:
Re–Ni/CeO_2
X-ray absorption near edge structure (XANES)
Electron withdrawing effect
WGS reaction
Oxygen vacancies

ABSTRACT

The catalytic activities of Re–Ni/CeO_2 bimetallic catalysts were investigated for the water gas shift reaction in the temperature range of 150–600 °C. Re–Ni/CeO_2 bimetallic catalysts were prepared by the incipient wetness impregnation method with aqueous solutions of $Ni(NO_3)_2{\cdot}6H_2O$ and NH_4ReO_4. The amount of Re was kept constant at 1 wt%, while that of Ni was varied at 1.0, 2.5, 5.0, 7.5 and 10.0 wt%. The activities of all doped samples were tested in a flow reactor with initial mixed feed gas of 5% CO and 10% H_2O. Re–Ni/CeO_2 bimetallic catalysts showed a higher rate of WGS reaction than Ni/CeO_2 monometallic catalysts. The results from XRD and Raman spectroscopy indicate that doped oxide species were dispersed on the ceria surface and H_2 chemisorption indicated better dispersion of Ni on the ceria surface with the addition of Re. X-ray absorption near edge structure (XANES) of the Ce L_3 edge indicated that Re promotes the reduction of Ce^{4+} at the surface and facilitates the WGS redox process. XANES results also indicated movement of electron density from Ni to Re leading to an enhancement of CO adsorption on the Ni active sites. All of these effects contributed to an increase of the WGS reaction rates.

1. Introduction

For clean energy production, pure hydrogen is required as a feed gas for electricity generation in a fuel cell. Hydrogen is generally produced by steam reforming of hydrocarbons and the reformate includes a small amount of some gases such as CO, CO_2, H_2O and CH_4. Among these impurities, CO is poisonous to the Pt electrode in the fuel cell and its concentration must be reduced before entering the fuel cell system. The water gas shift (WGS) reaction is normally employed since it can reduce the amount of CO to less than 1%.

The WGS reaction is described as follows:

$$CO + H_2O \leftrightharpoons CO_2 + H_2, \qquad H = -41.2\ \text{kJ/mol}$$

This reaction is moderately exothermic and the equilibrium conversion of CO decreases with increasing temperature, thus a catalyst is needed to keep a good conversion rate at a low temperature.

Cerium oxide (CeO_2) is widely used as a catalyst support because of its high oxygen storage capacity and reducibility [1–3]. Ceria plays the role of oxygen storage via the redox process ($Ce^{4+} \leftrightarrow Ce^{3+}$) by changing between oxygen storage (CeO_2) and oxygen release (Ce_2O_3) [4]. Many studies have shown that the addition of some metals onto the ceria support leads to an increase of catalytic activities for the WGS reaction [5–12]. It is know that noble metals such as Pt, Rh, Au, Pd, etc. are active for the WGS reaction. There are efforts underway to search for less expensive and more abundant metal promoters. Several studies have reported reasonable activities of transition metals such as Cu, Ni, Co, Fe, Mn, Mo on many supports for several reactions [13–19]. Among these metals, Ni has received much attention and has been employed as a promoter to enhance activities of many reactions. For example, Ni/CeO_2 for the reverse WGS reaction [20], Ni on Ce–Zr–O and ZrO_2–CeO_2–Al_2O_3 supports for reforming methane to synthesis gas [21,22], oxidation of methane with Ce–Ni–O mixed oxide catalyst [23], Ni on Ce–Zr–O, SiO_2, TiO2, MgO and activated carbon for carbon dioxide reforming of methane [24,25] and steam reforming of ethanol by using Ni on Al_2O_3 promotion with CeO_2 and ZrO_2 [26]. Some disadvantages are present when using Ni as a catalyst such as sintering of metallic and support phases [27,28]. The addition of other metals to form bimetallic catalysts such as Ni–Au, Ni–Cu, Ni–Rh and Ni–Pt are reported to lead to better dispersion of the metallic phase and slow down sintering of metallic and support phases [8,16,26,29]. Moreover, addition of the second metal also raises the catalytic activity.

Many research groups have reported that Re as a second metal can improve the activity of many reactions [30–34]. For the WGS reaction, Iida and Igarashi [35] compared the WGS activity of Pt–Re/TiO_2 (rutile) and Pt–Re/ZrO_2 and reported that Re promoted Pt dispersion and the state of Re could influence the catalytic activity. In conversion of glycerol by Pt–Re catalysts, the ability of Re to weaken the bonding of CO to the neighboring Pt sites was reported [36]. Pereira et al. used X-ray absorption near edge structure (XANES) to study the bonding of CO to bimetallic catalysts of Pt and other metals on carbon support. The electron withdraw-

* Corresponding author. Tel.: +66 43202222x12243; fax: +66 43202373.
E-mail address: sunhen@kku.ac.th (S. Hengrasmee).

0920-5861/$ – see front matter © 2011 Elsevier B.V. All rights reserved.
doi:10.1016/j.cattod.2011.05.022

ing effect by metals acting on the Pt d-orbitals led to a lowering of electron numbers that could provide back-donation to the CO molecules [37].

It is believed that the oxidation–reduction process is involved in the WGS mechanism and CeO_2 is usually used as a support for the WGS reaction due to its reducibility and high oxygen storage capacity. CeO_2 can store and release oxygen to undergo oxidation–reduction cycles and promotes catalytic activity of the reaction. Many studies have reported that doped metal can reduce ceria and increase its reducibility and oxygen storage capacity [10,38,39]. Sanchez and Gazquaz [40] proposed that oxygen vacancies in the fluorite structure of ceria alter the morphology and dispersion of the doped metal. Li and Fu [16], in studying the Cu and Ni-loaded CeO_2 catalyst for the WGS reaction, found that addition of both Cu and Ni increased the reducibility of ceria and purposed that the redox process of ceria is involved in the reaction mechanism.

In this paper, we studied the catalytic activities of Re–Ni/CeO_2 bimetallic catalysts for the WGS reaction. The catalysts were prepared by the incipient wetness impregnation method and characterized with standard methods such as X-ray diffraction (XRD), Raman spectroscopy, N_2 adsorption, H_2 chemisorption and H_2-temperature programmed reduction (H_2-TPR). The movement of electrons between Re and Ni was investigated by the XANES technique.

2. Experimental

2.1. Catalysts preparation

2.1.1. Preparation of CeO_2 support

The urea gelation method which is similar to those described by Kundakovic and Flytzani-Stephanopoulos [13] and Bickford et al. [41] was used for CeO_2 support preparation. Desired amounts of cerium nitrate hexahydrate ($Ce(NO_3)_3{\cdot}6H_2O$, 99%, Aldrich) and urea (H_2NCONH_2, 98%, Aldrich) were mixed in 100 mL of deionized water and the solution was heated to 100 °C under vigorous stirring. While the mixture was heated, 2 mL of ammonium hydroxide (NH_4OH, Aldrich) was added dropwise and yellow precipitates were obtained. The suspension was stirred and heated at the same temperature for 4 h to remove excess NH_3 and to age the precipitate. The suspension was filtered and washed twice with boiling deionized water. The filtered ceria precipitate was dried overnight at 110 °C and then calcined at 450 °C for 4 h.

2.1.2. Preparation of catalysts

Re–Ni/CeO_2 catalysts were prepared by the incipient wetness impregnation method with the use of aqueous solutions of ammonium perrhenate (NH_4ReO_4, 99%, Aldrich) and nickel(II)nitrate hexahydrate ($Ni(NO_3)_2{\cdot}6H_2O$, 98%, Carlo Erba). Different amounts of these metal salts were added dropwise onto prepared CeO_2 support. The amount of Re was kept constant at 1 wt% while that of Ni was varied in the order of 1.0, 2.5, 5.0, 7.5 and 10.0 wt%. The impregnated supports were dried overnight at 110 °C and then calcined at 650 °C for 8 h.

2.2. Catalysts characterization

2.2.1. Standard characterization

The structural properties of all doped catalysts were investigated by powder X-ray diffraction (XRD). XRD data were collected on a Bruker XRD D8 Advance GX 280 with Cu Kα radiation of wavelength 1.5406 Å. The diffractograms were recorded in the range of $2\theta = 20–80^\circ$ with scan speed and step size being 0.5 s/step and 0.02°, respectively. The crystalline size of the samples, d_{hkl}, were estimated from Scherrer's equation

$$d_{hkl} = \frac{0.9\lambda}{\mathrm{FWHM}\ \cos\theta} \quad (1)$$

where λ is the X-ray wavelength of Cu Kα radiation (1.5406 Å), FWHM is the broadening (in radians) at half-maximum of the (1 1 1) crystallographic plane which is the most intense peak and θ is the diffraction angle corresponding to the (1 1 1) plane. Lattice parameter (a) is calculated by Bragg's equation with the same crystallographic plane.

Nitrogen adsorption–desorption was obtained on a Autosorb 1-C instrument (Quantachrome) at −196 °C. The samples were degassed under vacuum at 300 °C for 3 h prior to nitrogen adsorption measurements. The specific surface areas of all catalysts were determined by the multipoint BET method.

H_2 chemisorption and % metal dispersion of all doped catalysts were determined by Quantachrome Autosorb 1-C instrument. The catalysts (200 mg) were first pretreated by Helium at 120 °C (rate 20 °C/min) for 30 min, then H_2 (99.999%, Thai Industrial Gas) was flowed over the sample while the temperature was raised at the rate of 20 °C/min to reach 350 °C and was kept at this temperature for 120 min. After pretreatment, the sample was cooled down under vacuum to room temperature (40 °C). The adsorbing gas (H_2) was sequentially added to the sample. The volume of hydrogen uptake (V) vs. equilibrium pressure (P/P_o) isotherm was plotted. The H_2 chemisorbed and percentage of metal dispersion can be calculated from this chemisorbed isotherm. The extrapolation method was used to obtain the volume of monolayer uptake (V_m). The monolayer of hydrogen uptake (N_m) which is expressed in micromole of hydrogen per gram of sample can be calculated by the following equation:

$$N_m = 44.61 V_m \quad (2)$$

V_m (cm^3/g) is determined by extrapolating the isotherm to zero pressure. The percent metal dispersion (D) can be estimated from the equation

$$D = \frac{N_m S M}{100 L} \quad (3)$$

where S is the adsorption stoichiometry of H_2 which is equal to 2, M and L are the molecular weight of loading metal and percent loading of the supported metal, respectively.

2.2.2. Raman spectroscopy

The Raman spectroscopy technique was used to observe the vibrational mode of prepared catalyst powder by using the Jobin Yvon T 64000 Raman spectrometer equipped with BX51 Olympus optical microscope. Charge couple device (CCD) was used to detect the vibrational signal, which was plotted as a function of wavenumber. The samples were irradiated by Ar ion laser with output power 30 mV and wavelength of 514.5 nm. The Raman spectra were collected in the range of 200–2000 cm^{-1}.

2.2.3. Temperature programmed reduction (TPR)

H_2-temperature programmed reduction profiles of doped catalysts were obtained from Autosorb 1-C instrument (Quantachrome). The samples (200 mg) were first pretreated by helium at 120 °C (rate 10 °C/min) to clean up the sample for 30 min. After pretreating with helium, 5% H_2 in 95% N_2 ($H_2 = 5.3 \pm 0.2\%$, Thai Industrial Gas) was flowed at a rate of 80 ml/min over the pretreated sample while the temperature was raised from 40 °C to 1000 °C at the rate of 10 °C/min. The changes in thermal conductivity were analyzed with TCD detector and H_2-consumption was calculated and plotted as a function of temperature.

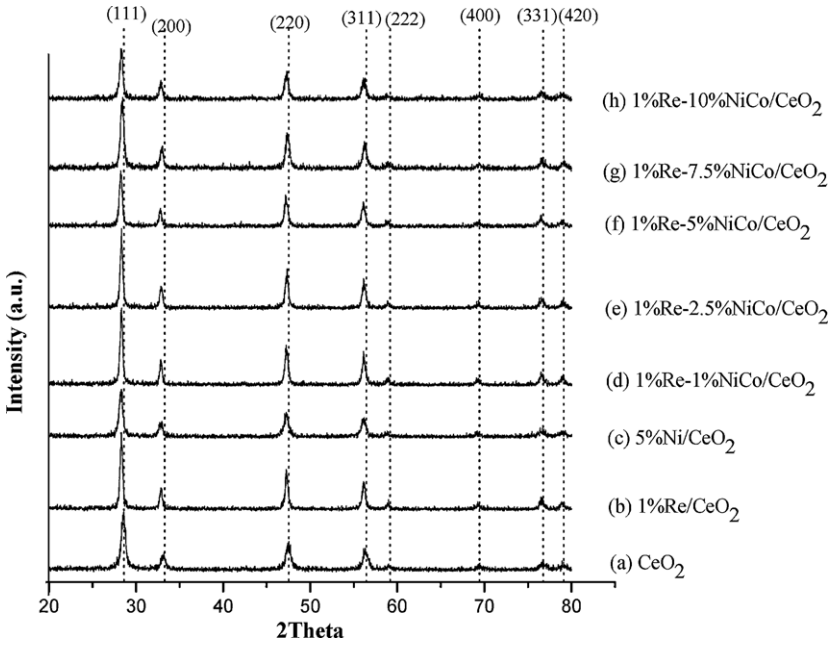

Fig. 1. XRD patterns of (a) CeO_2, (b) 1% Re/CeO_2, (c) 5% Ni/CeO_2 and (d)–(h) 1% Re–*X*% Ni/CeO_2 (*X* = 1.0, 2.5, 5.0, 7.5 and 10.0) catalysts.

2.3. Water gas shift catalytic activities test

The water gas shift (WGS) catalytic activity test for all catalysts was carried out in a flow reactor in the temperature range of 150–600 °C. Appropriate amounts of catalysts (20 mg, 14.5 nm in size) were loaded between the two layers of quartz wool in the quartz tube reactor (0.6 cm ID, 0.8 cm OD × 30 cm length). The quartz tube was placed inside the temperature controllable tube furnace. The temperature was monitored by K-type thermocouple that was placed at the top of the catalyst bed. The initial feed gas of CO (5 ml/min) and He (85 ml/min) was flowed into a water-saturator in which the temperature was kept at 47 °C to pick up the desired amount of water vapor. Thus the mixed feed gas, 5% CO, 10% H_2O and balance He, was allowed to pass through the catalyst bed of the reactor. The flows of feed gases were controlled by mass flow controller (Dywer). Both temperature and flow rate were monitored by Data Logger Wisco DL2100B. The experiment was carried out at atmospheric pressure. The catalysts were pretreated at 120 °C under reactant stream for 90 min. The test procedure for the WGS reaction was a stepwise change with increase of temperature only upward. The catalysts were kept at each temperature for 60 min. The reactant gas (CO) and product gas (CO_2) were analyzed by on-line gas chromatography (Agilent 6890N Series, Agilent technology) equipped with HAYESEP D Packed Column and TCD detector. The water was trapped out before the gas mixture entered the GC. The percent conversion of CO was plotted as a function of temperature. The CO conversion (X_{CO}) was calculated by the following expression

$$X_{CO} = \frac{C_{CO}^{in} - C_{CO}^{out}}{C_{CO}^{in}} \quad (4)$$

The rates of reaction were measured in a separate experiment which was performed under differential conditions, where the conversion of reactants was lower than 10% and with this condition heat and mass transfer effects were negligible. The rates were calculated by the following expression

$$r_{CO} = \frac{F_{CO}X_{CO}}{W_{cat}} \quad (5)$$

where r_{CO} is the conversion rate of CO (mol/g s), F_{CO} is the molar flow rate of CO into the reactor (mol/s), and W_{cat} is the mass of the catalysts (g). The r_{CO} reported in this manuscript is an average of three reproducible experiments.

2.4. X-ray absorption spectroscopy

X-ray absorption spectroscopy measurements were made in the X-ray absorption near edge structure (XANES) region on Beamline 8 at the Synchrotron Light Research Institute (SLRI), Nakhonrachasima, Thailand [42]. The electron storage ring was operated at 1.2 GeV. The fixed-exit double crystal monochromator (DCM) which employed two parallel InSb (1 1 1) and Ge (2 2 0) crystals for low and high energy range were used as synchrotron radiation selection. The monochromatic flux at the sample was 10^8–10^{10} photons/s. The ion chambers were filled with a mixture of nitrogen and helium for Re M_5 absorption measurement and with a mixture of argon and helium for Ce L_3 and Ni K absorption edge measurements. These chambers were installed in front of and behind the sample which continuously detected the incident (I_o) and transmitted (I_1) X-ray beam. A Lytle detector was used to detect sample fluorescence. The spectra were recorded in fluorescence mode for Re M_5 and Ni K absorption edges and transmission modes for Ce L_3 absorption edge. In each measurement, the sample was spread onto the Kapton window which was stuck on the sample frame and energy was scanned at 30 eV below and 90 eV above, the edge energy with a step size of 0.2 eV. Data reduction was carried out by pre-edge background removal and normalization by division of the height of the absorption edge. The software Athena was used to process the data reduction.

3. Result and discussion

3.1. Standard characterization

XRD patterns of CeO_2, Ni/CeO_2 and Re–Ni/CeO_2 with different metal loading are presented in Fig. 1. All doped samples exhibit the diffraction peak which corresponds to the fluorite structure of CeO_2. Both rhenium oxide and nickel oxide were not observed in

Table 1
Specific surface area, crystalline size, lattice constant, H_2 chemisorbed and % dispersion of various catalysts.

Sample	S_{BET} (m^2/g)	Crystalline size[a] (nm)	Lattice constant[a] (nm)	H_2 chemisorbed (μmol/g)	% dispersion
CeO_2		68.3	14.2	0.541	–
1% Re/CeO_2	26.8	22.6	0.547	–	–
5% Ni/CeO_2	33.8	18.6	0.546	25.5	6.0
1% Re–1% Ni/CeO_2	25.2	26.1	0.546	32.3	38
1% Re–2.5% Ni/CeO_2	26.6	27.0	0.545	44.5	21
1% Re–5% Ni/CeO_2	29.0	22.0	0.547	50.6	12
1% Re–7.5% Ni/CeO_2	29.7	20.6	0.545	60.5	10
1% Re–10% Ni/CeO_2	30.9	19.1	0.547	71.0	8.3

[a] Calculated from the (1 1 1) crystallographic plane.

all doped samples, indicating that these oxide species are finely dispersed on the ceria surface [30,43]. Based on Bragg's equation, the lattice parameters of ceria and doped catalysts were calculated from (1 1 1) crystallographic planes. For pure CeO_2 support, the lattice parameter is found to be 0.541 nm which is in agreement with other works [10,44]. The lattice parameter of other catalysts (Re/CeO_2, Ni/CeO_2 and Re–Ni/CeO_2) also displayed similar values in the range of 0.0545–0.0547 nm. From these result, it can be concluded that addition of Ni or Re did not lead to modification of the ceria bulk structure.

Table 1 summarizes the results from particle analysis and XRD. The BET surface area of CeO_2 is 68.3 m^2/g which is similar to other studies [13,16,45]. Lowering of the surface area and increasing of crystalline size of the doped samples are believed to be a consequence of sintering at the higher calcination temperature.

The results from H_2 chemisorption and % active metal dispersion are also displayed in Table 1. The data on H_2 chemisorption and % active metal dispersion are referred to Ni metal since H_2 did not adsorb on 1% Re/CeO_2. The % metal dispersion results indicate that Re helped to disperse Ni metal on the ceria support. However, the dispersion decreased with an increase of Ni content. The reduction of the metal dispersion is the result of the agglomeration and growth of metal-ceria crystallites at high calcination temperature. As the results of better metal dispersion, the H_2 chemisorption increased.

3.2. Raman spectroscopy

Raman spectroscopy is another useful tool to obtain additional structural information of oxide catalysts that exhibit lattice disorder. For ceria with fluorite structure, the only Raman active mode is F_{2g} which appears at 464 cm^{-1}[46]. This vibration mode is a symmetric vibration of 8 oxygen atoms around each ceria cation. Replacement of Ce^{4+} by another metal ion of similar size but different charge would lead to shifting and lowering of the F_{2g} Raman active band of CeO_2 together with the appearance of a small additional peak due to vibration of oxygen around the adatom [47]. Fig. 2 displays the Raman spectra of ceria and doped Re–Ni/CeO_2 catalysts. It is clearly seen that only F_{2g} Raman modes of ceria are present without small additional peaks nearby. Due to high metal dispersion at the surface the intensity of this peak decreases with metal contents. From these results it can be concluded that the doped metals (Ni and Re) are not incorporated into the ceria lattice and the metal oxides only reside on the surface of the ceria support.

The small broad peaks beside the main Raman active peak located at 553 and 630 cm^{-1} are assigned to be due to the presence of NiO. Several studies have reported only one Raman symmetric stretching mode of Ni–O in NiO at 550 cm^{-1} [48,49]. Srnbnek et al. [50] while studying a NiO_x film on alumina reported the Raman spectra of NiO_x species. They found that increasing O_2 in the film preparation process led to shifting of the broad peak to 560–650 cm^{-1} and this position was assigned to the Ni_2O_3 species.

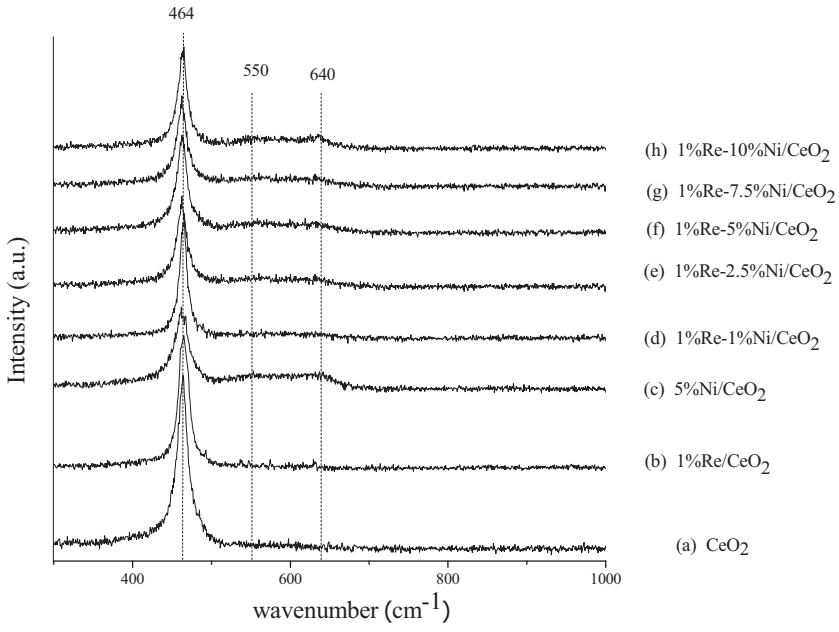

Fig. 2. Raman spectra of (a) CeO_2, (b) 1% Re/CeO_2, (c) 5% Ni/CeO_2 and (d)–(h) 1% Re–*X*% Ni/CeO_2 (*X* = 1.0, 2.5, 5.0, 7.5 and 10.0) catalysts.

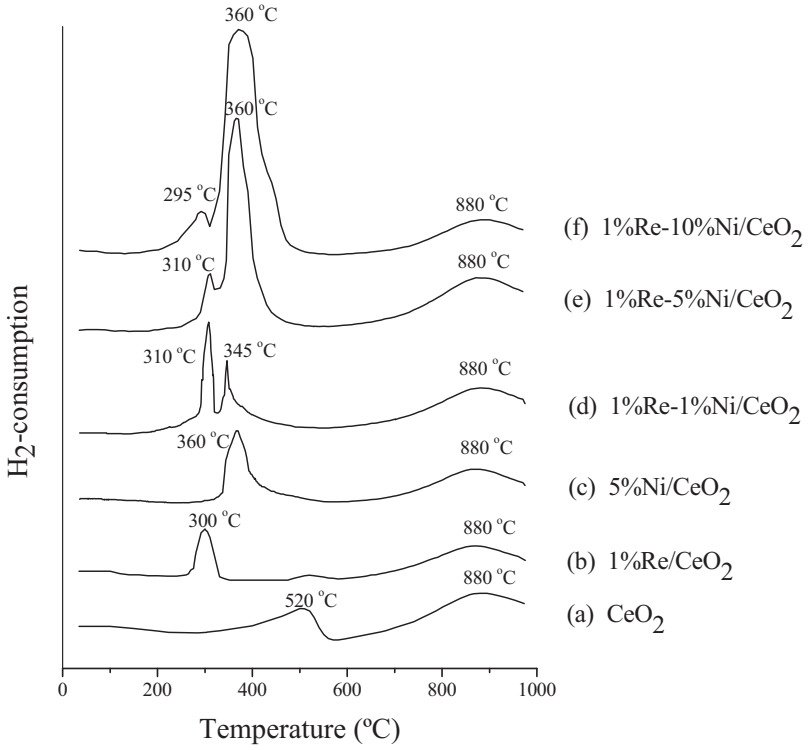

Fig. 3. H_2-TPR profiles of (a) CeO_2, (b) 1% Re/CeO_2, (c) 5% Ni/CeO_2 and (d)–(f) 1% Re–*X*% Ni/CeO_2 (*X* = 1.0, 5.0 and 10.0) catalysts.

Our spectra indicate the present of Ni^{2+} (as NiO) and a small amount of Ni^{3+} (as Ni_2O_3) on the surface of ceria. Due to very low content of Re, the Re–O vibration band was not observed.

3.3. H_2-temperature programmed reduction

The H_2-TPR profile of CeO_2 and all doped catalysts are illustrated in Fig. 3. There are two main reduction peaks of ceria support. The first one is located at 520 °C which is attributed to reduction of the uppermost layer of Ce^{4+} to Ce^{3+} and another one at 880 °C is assigned to reduction of bulk ceria [51].

Addition of Re and Ni onto ceria brought up additional reduction peaks around 295–360 °C. In the case of Re/CeO_2, the reduction peak at 300 °C appears which is due to the reduction of rhenium oxide [52], while another peak at 530 °C is due to CeO_2. It is not clear what the final state of Re is after the reduction since it seems to depend on the state of the supports. For examples, Johnson and Leroy [53] reported that rhenium on alumina is reduced exclusively by hydrogen to the Re^{4+} state. In contrast, Webb [54] reported that alumina supported rhenium is completely reduced at 400 °C. Extensive study is required in order to determine the final state of Re/CeO_2 upon hydrogen reduction. For Ni/CeO_2, a low temperature reduction peak appears as a rather broad peak at 360 °C. This peak is assigned to reduction of Ni^{2+} to Ni^0 and a concurrent reduction of surface ceria. This type of effect is well known for metal/ceria catalysts and is usually attributed to spill over of hydrogen atoms produced by dissociation of H_2 on metal particles. This reduction temperature has been reported to vary in different works. Wang et al. reported the reduction temperature of Ni/CeO_2 at 320 °C, while other works on the same catalyst reported it at 340–420 °C [55–58]. The difference in the reduction temperature is concluded to be dependent on the interaction between the NiO and the ceria support.

The TPR profile of $Re–Ni/CeO_2$ catalysts displays two reduction peaks in the low temperature range. The first reduction temperature is located around 295–310 °C which is due to the reduction of rhenium oxide species. Another peak at 345–360 °C is assigned to reduction of NiO and surface ceria. The peak area increases with an increase of Ni. The temperature for maxima of the peaks for reduction of the bimetallic catalysts ($Re–Ni/CeO_2$) remained relatively unchanged when compared with the reduction temperatures of the monometallic catalysts (Ni/CeO_2 and Re/CeO_2). This result indicated that the two oxide phases are separate. When the nickel oxide reduction peak of 5% Ni/CeO_2 and 1% Re–5% Ni/CeO_2 are compared, it is clearly seen that 1% Re–5% Ni/CeO_2 displayed higher H_2 consumption than 5% Ni/CeO_2. This result indicated better dispersion of nickel oxide on the surface due to the presence of 1% Re.

3.4. WGS catalytic activities

The results of WGS activities of monometallic (Ni/CeO_2) and bimetallic ($Re–Ni/CeO_2$) catalysts are presented in Fig. 4a where the conversion of CO is plotted as a function of temperature. The equilibrium conversion is also displayed for comparison. It is observed that Re–Ni bimetallic catalysts shift the conversion curves toward lower reaction temperature (lines d-h) while the conversion curves of monometallic catalyst Ni/CeO_2 appears at higher reaction temperature (line c). The $Re–Ni/CeO_2$ bimetallic catalysts give measurable WGS conversion at temperatures above 220 °C and the conversion of CO increases with increasing temperature and reaches equilibrium at 400 °C. The WGS activity of CeO_2 and 1% Re/CeO_2 are also plotted for comparison (lines a and b) and it is clearly seen that these catalysts are not very active for the WGS reaction.

Preliminary investigation of the effect of Re on Ni/CeO_2 was performed by variation of Re loading (1, 2 and 5 wt%) while the Ni loading was kept constant at 5 wt% (Table 2). The results show that an increase of Re content did not significantly alter the WGS catalytic activities. Therefore, the loading amount of Re was kept constant at 1 wt%. Fig. 4a (line d–h) displays the effect of increasing the Ni content of the bimetallic catalysts. The conversion curve shows that 1% Re–10% Ni/CeO_2 gives the highest measurable

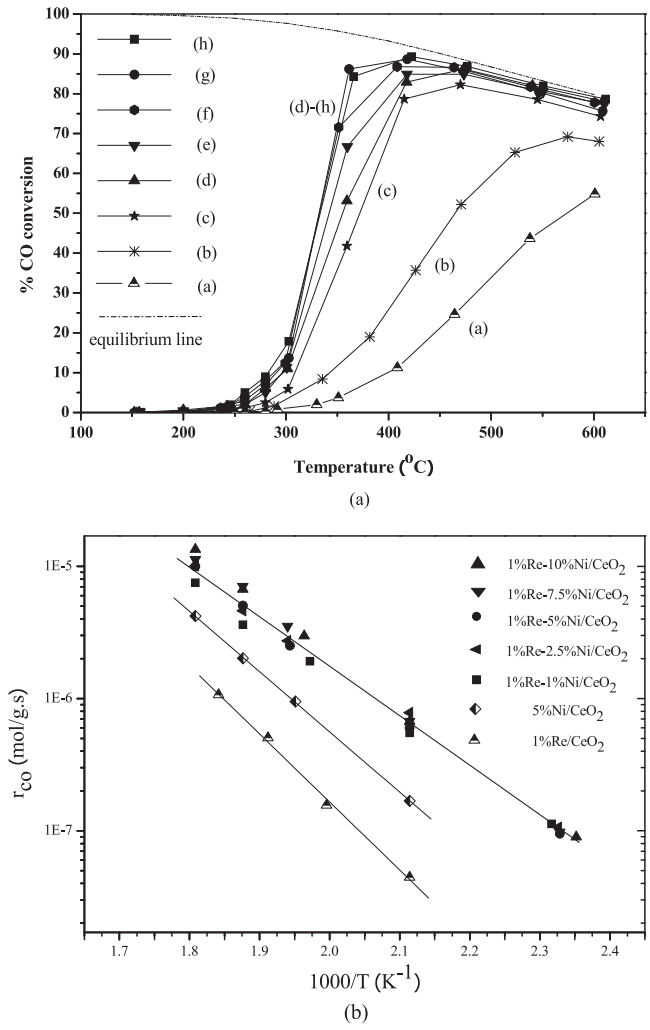

Fig. 4. (a) WGS catalytic activities of (a) CeO_2 (b) 1% Re/CeO_2, (c) 5% Ni/CeO_2, and (d)–(h) 1% Re–*X*% Ni/CeO_2 (*X* = 1.0, 2.5, 5.0, 7.5 and 10.0) catalysts. (b) Arrhenius plot of reaction rates over CeO_2, 1% Re/CeO_2, 5% Ni/CeO_2 and 1% Re–*X*% Ni/CeO_2 (*X* = 1.0, 2.5, 5.0, 7.5 and 10.0) catalysts.

conversion at temperatures over 220 °C and the reaction reaches equilibrium at 390 °C.

The Arrhenius plots of various Re–Ni/CeO_2 ratios are illustrated in Fig. 4b. It is obvious that the specific rate (per gram of catalyst) of bimetallic catalysts at 300 °C is higher than that of monometallic catalysts. The rates of CO conversion at 300 °C of all doped catalysts are summarized in Table 2. The rates of WGS reaction on bimetallic catalysts are almost twice the rate on monometallic catalysts. For example, the rates at 300 °C are 20.1 μmol/g s for 1% Re–5% Ni/CeO_2, 10.1 μmol/g s for 5% Ni/CeO_2, and 2.80 μmol/g s for 1% Re/CeO_2. These numbers indicate that the rate for the bimetallic catalyst is not a combined catalytic effect of Ni and Re metals. There should be other factors that contribute to the increase of the WGS rate upon addition of Re. When the WGS rates of the bimetallic catalysts with different contents of Ni are compared, it appears that the rate increased with an increase of Ni. The rate slowly increased from 18.5 μmol/g s for 1% Re–1% Ni/CeO_2 to 30.0 μmol/g s for 1% Re–10% Ni/CeO_2. The increase in WGS rate of the bimetallic catalyst with the increase of Ni content corresponds well with the results from H_2 chemisorption. A trial plot (not shown in this manuscript) of the WGS rate vs. the hydrogen chemisorption data showed reasonably good correlation between the number of exposed Ni and the reaction rate for the different catalysts, Re monometallic, Ni monometallic and Re–Ni bimetallic.

Table 2
The rate of reaction at 300 °C and apparent activation energy (E_a) for all doped catalysts.

Sample	Rate at 300 °C (μmol/g s)	E_a (kJ/mol)
1% Re/CeO_2	2.80	91
5% Ni/CeO_2	10.1	88
1% Re–5% Ni/CeO_2	20.1	73
2% Re–5% Ni/CeO_2	23.2	73
5% Re–5% Ni/CeO_2	22.5	73
1% Re–1% Ni/CeO_2	18.5	77
1% Re–2.5% Ni/CeO_2	19.0	76
1% Re–5% Ni/CeO_2	20.1	73
1% Re–7.5% Ni/CeO_2	22.9	73
1% Re–10% Ni/CeO_2	30.0	71

The apparent activation energy of the WGS reaction was obtained from the slopes of the Arrhenius plots in Fig. 4b and the results are also summarized in Table 2. The apparent activation energy of the WGS reaction on Ni/CeO_2 is 88 kJ/mol while that on Re–Ni/CeO_2 is around 71–77 kJ/mol. The difference in apparent activation energy is attributed to the effect of added Re. Lowering of apparent activation energy in Re–Ni/CeO_2 corresponds well with the increasing WGS reaction rate. Qi and Flytzani-Stephanopoulos [7] in studying the WGS reaction also reported lowering of the apparent activation energy of Ce(La)Ox upon doping with Cu, and they suggested different pathways of the two catalysts. Upon investigating the apparent activation energy of the bimetallic catalysts with different Ni contents, it appeared that the activation energies also slightly decreased with an increase of Ni content. Therefore, under this experimental condition Ni plays a role in the rate limiting step. The calculated activation energies in this study are in agreement with other reports for WGS reactions with various metals on ceria support [10,59,60].

3.5. X-ray absorption near edge structure (XANES)

It is interesting to investigate the role of Re in increasing the WGS reaction rate of the Ni/CeO_2 catalyst. There are many elementary steps that are involved in WGS reaction such as oxidation–reduction at the surface, adsorption–desorption of the adsorbed species. All of these processes are controlled by the availability of electrons at the support surface. Therefore, it is needed to investigate the availability of surface electrons on the support. X-ray absorption spectroscopy (XAS) is a powerful technique for studying the electronic nature of substance. In the XAS technique, the intense X-ray beam is used to excite the electrons in core levels of the probe atoms into an unoccupied valence shell. Analyzing the XANES spectra will provide information on oxidation states and the valence shell electronic population [61]. The XANES technique was employed in our study to investigate the oxidation state and d-electron density of metals in our catalysts. It is worth mentioning that in the XANES study, a high content of metal under study is needed in order to obtain reasonable spectra since this technique is not sensitive if the metal content is low. Therefore, the metal contents used in XANES studies were higher than the contents of metals in the catalysts study.

3.5.1. Oxidation state of Ce

XANES spectra of Ce L_3 absorption edges of standards (Ce metal, $Ce(NO_3)_3{\cdot}6H_2O$, and CeO_2) and doped samples (1% Re/CeO_2, 5% Ni/CeO_2, and 1% Re–5% Ni/CeO_2) are illustrated in Fig. 5a. The XANES spectra of cerium standard $Ce(NO_3)_3{\cdot}6H_2O$ exhibits a single white line located at 5725.5 eV. This peak characterizes the Ce in the trivalent state and it is the dipole-allowed transition of Ce 2p to the Ce 4f15d state [62]. In the case of CeO_2, there are two main

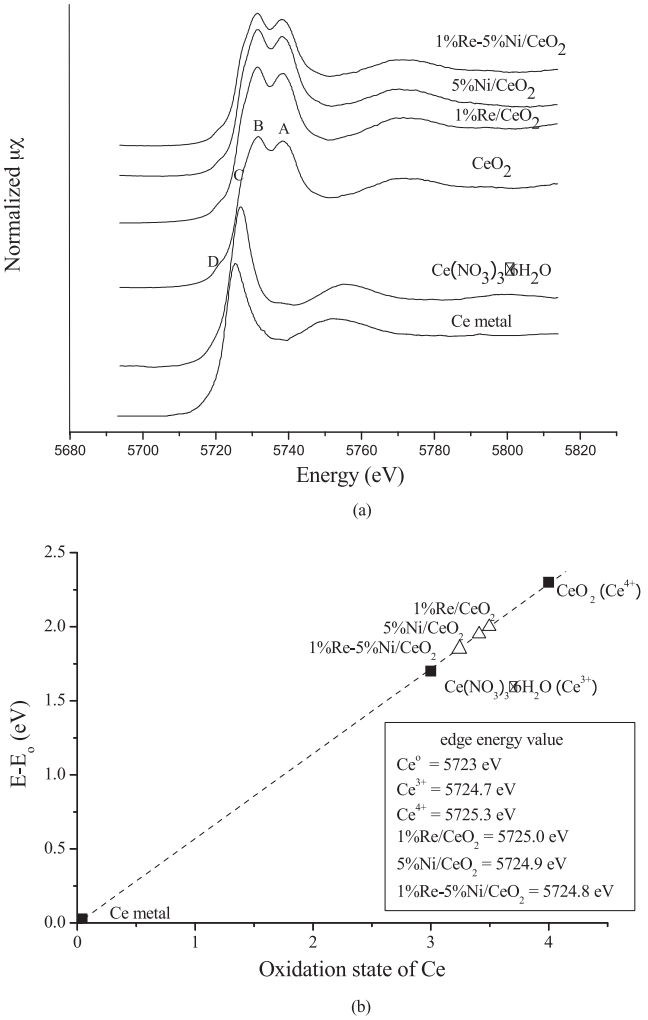

Fig. 5. (a) XANES spectra of the Ce L_3 absorption edge for Ce metal (Ce^0), $Ce(NO_3)_3{\cdot}6H_2O$ (Ce^{3+}), CeO_2 (Ce^{4+}), 1% Re/CeO_2, 5% Ni/CeO_2 and 1% Re–5% Ni/CeO_2. (b) Relationship between edge energy shift of Ce compounds and the oxidation states. Filled squares are Ce^0, $Ce(NO_3)_3{\cdot}6H_2O$ (Ce^{3+}) and CeO_2 (Ce^{4+}) standards, open triangles are 1% Re/CeO_2, 5% Ni/CeO_2 and 1% Re–5% Ni/CeO_2.

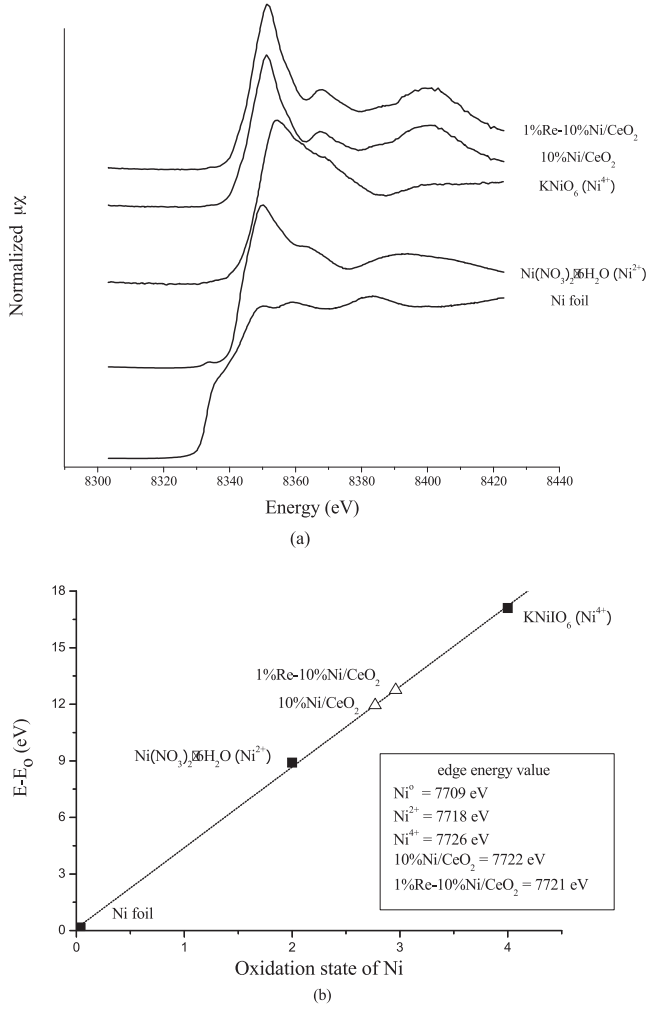

Fig. 6. (a) XANES spectra of the Ni K absorption edge for Ni foil (Ni^0), $Ni(NO_3)_2{\cdot}6H_2O$ (Ni^{2+}), $KNiO_6$ (Ni^{4+}), 10% Ni/CeO_2 and 1% Re–10% Ni/CeO_2. (b) Relationship between edge energy shift of Ni compounds and the oxidation states. Filled squares are Ni^0, $Ni(NO_3)_3{\cdot}6H_2O$ (Ni^{2+}) and $KNiO_6$ (Ni^{4+}) standards, open triangles are 10% Ni/CeO_2 and 1% Re–10% Ni/CeO_2.

peaks that are usually observed. The high-energy peaks A and B were assigned to the transition of Ce 2p to a mixed valence state of cerium, one with electron configuration of $4f^0$ and another one with $4f^1$ [63]. Besides these two peaks, some additional small peaks were also observed. The low energy shoulder (peak C) was due to the crystal field splitting of the Ce 5d state for bulk ceria or was assigned to a Ce^{3+} impurity [62]. The pre-edge peak D was the result of transition of the unoccupied Ce d-state at the bottom of the CeO_2 conduction band or that of the dipole-forbidden from $2p_{3/2}$ to 4f [64]. Our XANES spectra of Ce L_3 edge for 1% Re/CeO_2, 5% Ni/CeO_2, and 1% Re–5% Ni/CeO_2 contain features that are similar to the CeO_2 spectra.

In studying the XANES spectra, the linear relationship between the oxidation state and the edge energy shift of the element has been reported [65,66]. Edge energy is the energy that is required to excite the core electron to an unoccupied valence band and in order to obtain this energy the first derivative of the spectra at the energy jump is taken. Fig. 5b illustrates the Ce L_3 edge energy of 1% Re/CeO_2, 5% Ni/CeO_2, 1% Re–5% Ni/CeO_2, $Ce(NO_3)_3{\cdot}6H_2O$ and CeO_2 relative to the edge energy of Ce^0. A linear fit was constructed through L_3 energy shift of Ce^0, Ce^{3+} and Ce^{4+}. The edge energy shifts of 1% Re/CeO_2, 5% Ni/CeO_2 and 1% Re–5% Ni/CeO_2 relative to Ce^0 were placed on this linear fitting line at appropriate values of edge energy shift (ΔE) and the apparent oxidation state of Ce in all samples appears to be between +3 and +4. This result indicates the coexistence of Ce^{3+} and Ce^{4+} in which Ni reduced Ce^{4+} in CeO_2 by transferring electron density into a d-orbital of Ce^{4+}, leading to a small amount of Ce^{3+}. Re also reduced Ce^{4+} in CeO_2 but the extent of the reduction was lower. Evidence for electrons density transfer from Ni will be shown by the increasing of the Ni oxidation state in the next part. Among these three catalysts, the oxidation state of Ce in 1% Re–5% Ni/CeO_2 was the lowest. This result seems to indicate that Re assists Ni in reducing Ce^{4+} leading to more Ce^{3+} at the ceria surface.

3.5.2. Oxidation state of Ni and Re

The plot of XANES spectra of K absorption edge of Ni standards (Ni^0 from Ni foil, Ni^{2+} from $Ni(NO_3)_2{\cdot}6H_2O$, and Ni^{4+} from $KNiO_6$) and Ni catalysts (10% Ni/CeO_2 and 1% Re–10% Ni/CeO_2) are displayed in Fig. 6a. Edge energy shift of Ni^{2+} and Ni^{4+} relative to Ni^0 is plotted in Fig. 6b. A linear fit was constructed through K absorption edge energy of Ni^0, Ni^{2+} and Ni^{4+}. The edge energy shifts of 10% Ni/CeO_2 and 1% Re–10% Ni/CeO_2 were placed on this straight line and it was found that the oxidation state of Ni in these samples was higher than +2. For 10% Ni/CeO_2, the oxidation state of Ni is close

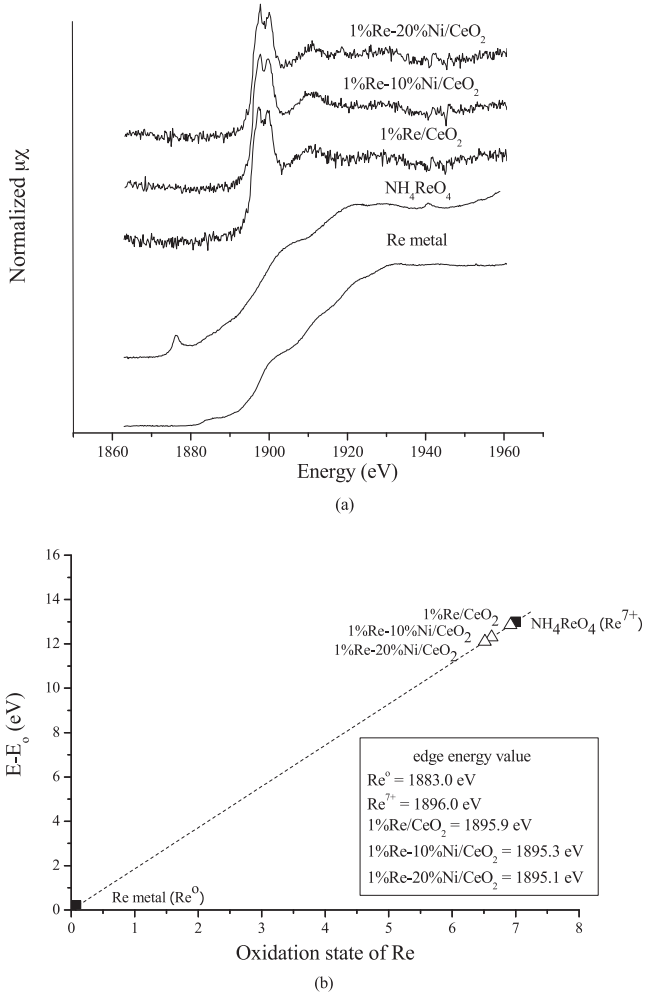

Fig. 7. (a) XANES spectra of the Re M_5 absorption edge for Re metal (Re^0), NH_4ReO_4 (Re^{7+}), 1% Re/CeO_2, 1% Re–10% Ni/CeO_2 and 1% Re–20% Ni/CeO_2. (b) Relationship between edge energy shift of Re compounds and the oxidation states. Filled squares are Re powder (Re^0) and NH_4ReO_4 (Re^{7+}) standard, open triangles are 1% Re/CeO_2, 1% Re–10% Ni/CeO_2 and 1% Re–20% Ni/CeO_2.

to +3 indicating the electron movement from Ni^{2+} to Ce^{4+} leading to increase of the Ni^{2+} oxidation state and lowering of the Ce^{4+} oxidation state. For 1% Re–10% Ni/CeO_2, the oxidation state of Ni was further increased to be a little above +3. This indicates that more electrons were moved out from Ni^{2+} and these results confirm that Ni donates its electrons to both Ce^{4+} and Re^{7+}.

Fig. 7 displays XANES spectra and a plot of edge energy shift of Re M_5 absorption edges. The standards are Re metal (Re^0), and NH_4ReO_4 (Re^{7+}). The catalysts are 1% Re/CeO_2, 1% Re–10% Ni/CeO_2, and 1% Re–20% Ni/CeO_2. A linear relationship between M_5 edge energy shift of Re^0 and Re^{7+} was constructed in Fig. 7b. Many papers report a linear correlation between Re valence and its edge energy shift with respect to Re metal [36,66], and therefore we are confident in drawing a straight line through the M_5 absorption edge of Re with the two standards (Re^0 and Re^{7+}). The edge energies of 1% Re/CeO_2, 1% Re–10% Ni/CeO_2 and 1% Re–20% Ni/CeO_2 were placed on this straight line and it appears that the oxidation states of Re in these samples are lower than +7. Since the catalysts were calcined in air, their oxidation state should be close to the precursor salt (NH_4ReO_4:Re^{7+}). Lowering of Re oxidation state indicates that electrons were moved into Re d-orbitals.

The results from oxidation states of all metals (Ce, Ni and Re) indicate that Ni donated electrons to both CeO_2 and Re in the catalysts leading to lowering of Re and Ce oxidation states and increasing of the Ni oxidation state.

To further confirm the electron movement among the metals in the catalysts, the white line intensities of Re and Ni in the catalysts were compared. The white line intensity is related to occupancy or electron density in the d-state of the element. Higher electron density means that fewer electrons can be raised up into its d-state, and therefore the intensity of the white line is low. In contrast, lower density of electrons in the d-state leads to more excitable electrons, so a higher number of photons are required to excite electrons and the white line is strong. Fig. 8a compares the white line of the Re M_5 absorption edge for 1% Re in the vicinity of 10% and 20% Ni (rather high contents of Ni are required for clarity). The amount of Ce in all samples was kept constant to eliminate the electron withdrawing effect of Ce. It is seen that the white line intensity of 1% Re with 10% Ni is a little higher than that with 20% Ni which indicates that Re in the vicinity of 10% Ni has lower d-electron density than Re with 20% Ni. This comparison indicates that 10% Ni donates less d-electron density to Re than 20% Ni does. On the other hand, Fig. 8b presents the white line of the Ni K absorption edge for 10% Ni in the vicinity of 1% Re and 10% Re. The higher peak belongs to 10% Re, which also indicates that Ni with 10% Re has lower d-electron density than Ni with 1% Re. This result indicates that higher Re content withdraws more electron density from Ni. These results confirm that electron density was transferred from Ni to Re. The XANES spectra of Re in Fig. 8a has rather high background due to limitations of the instrument. The experiment was carried out on the Re M_5 absorption edge which has quite low energy. However, six spectra were averaged and care was taken in placing the pre-edge and post-edge of the spectra at the same position. Although the differences of the white line intensities were low, the direction of electron density transfer indicated by the white line intensities corresponds well with the information of oxidation states of Re and Ni. The changes of oxidation states and white line intensity comparison for Re and Ni lead to the conclusion that electrons are transferred from Ni to Re leading to increase of Ni oxidation state and lowering of electron density in the d-state of Ni.

3.5.3. The role of Re in enhancing WGS reaction activity of Ni/CeO_2

It seems that there are many factors that contribute to the high WGS activity of bimetallic Re–Ni on ceria. The dependences of the WGS rate and the apparent activation energies on Ni contents indicate that Ni has an important role in the rate determining step. The agreement between the increases of WGS rate of the bimetallic catalysts with higher H_2 chemisorption shows that Re helps to disperse Ni oxide on the ceria surface. Apart from better metal dispersion, movement of electron density among the three metals seems to have an important effect. Several studies have reported that the WGS mechanism involves the redox mechanism on the ceria surface [5,67,68]. XANES results indicate that Ni reduces Ce^{4+} at ceria surface to Ce^{3+} and the creation of Ce_2O_3 at the surface leads to the production of oxygen vacancies that improve the mobility of electrons at the surface. Addition of Re promotes the reduction of Ce^{4+} at the ceria surface. This result is in agreement with the TPR profile which shows the surface reduction peak of the bimetallic catalysts to be at a temperature lower than the ceria reduction temperature (520 °C). Another result that is obtained from the XANES study is the withdrawing of electron density from Ni to Re. As a result of the electron withdrawing effect, the d-electron density of Ni is lowered and donation of electron density from the CO lone pairs to Ni d-orbital would be favored. Easier adsorption of CO together with better dispersion of nickel oxide (also promoted by the presence of Re) would lead to faster WGS rate.

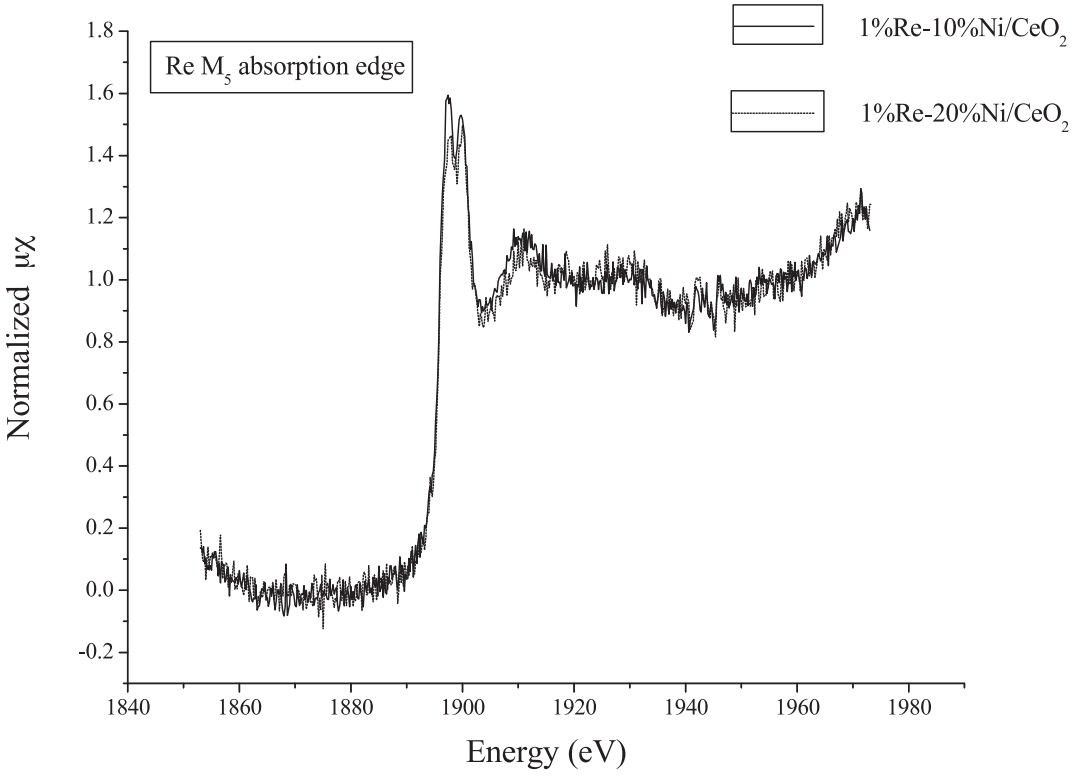

(a)

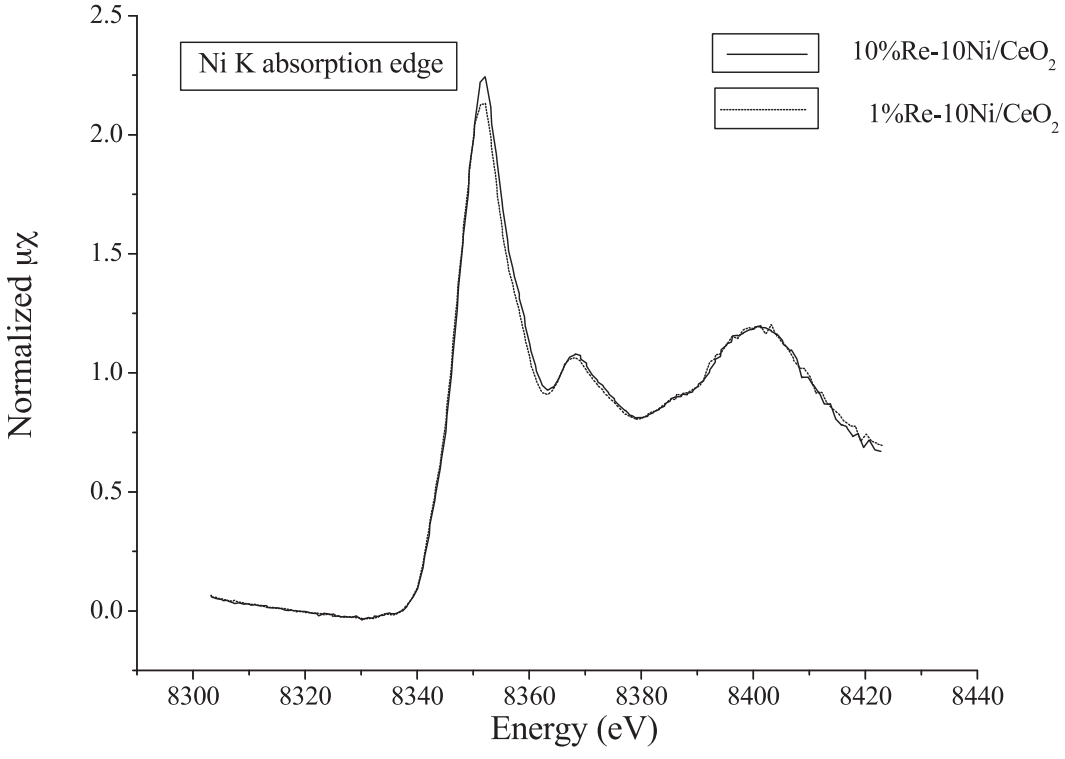

(b)

Fig. 8. (a) Comparison of white line intensity of Re M_5 absorption edge for 1% Re–10% Ni/CeO_2 and 1% Re–20% Ni/CeO_2. (b) Comparison of white line intensity of Ni absorption edge for 1% Re–10% Ni/CeO_2 and 10% Re–10% Ni/CeO_2.

4. Conclusion

Re–Ni/CeO_2 bimetallic catalysts were studied for the catalytic activity of the water gas shift reaction. Re–Ni/CeO_2 bimetallic catalysts showed higher catalytic activity than monometallic Ni/CeO_2 and the reaction rates depend on the content of Ni. The results from XRD and Raman spectroscopy indicate that oxide species of added metals are dispersed on the ceria surface. H_2-TPR profiles show that Ni lowers the surface reduction temperature of ceria through the spill over of the hydrogen atoms. X-ray absorption near edge structure (XANES) was used to describe the role of added metals in enhancing WGS activity. The XANES spectra of the Ce L_3 absorption edge indicate that Re facilitates the electron movement on the ceria surface by promoting the reduction of the surface ceria and increasing the oxygen vacancies. The XANES spectra of Re M_5 absorption edge and Ni K absorption edge indicate transfer of d-electron density from Ni to Re leading to easier adsorption of Co onto the Ni active sites.

In summary, it seems that Re influences the catalyst performance in several ways. Re increases the reducibility of the surface ceria, and facilitates the redox process at the surface. Re also increases the metal active sites and promotes CO adsorption in the Ni active sites. All of these effects contribute to an increase in the WGS reaction rates.

Acknowledgements

Our research group would like to thank the Center for Innovation in Chemistry (PERCH-CIC), Commission on Higher Education, Ministry of Education and the National Nanotechnology Center, National Science and Technology Development Agency for financial support. Generous beam time from the Synchrotron Light Research Institute (SLRI) is also gratefully acknowledged.

References

[1] C. de Leitenburg, A. Trovarelli, J. Llorca, F. Cavani, G. Bini, Appl. Catal. A: Gen. 139 (1996) 161–173.
[2] A. Martinez-Arias, M. Fernandez-Garcia, L.N. Salamanca, R.X. Valenzuela, J.C. Conesa, J. Soria, J. Phys. Chem. B 104 (2000) 4038–4046.
[3] E. Mamontov, T. Egami, R. Brezny, M. Koranne, S. Tyagi, J. Phys. Chem. B 104 (2000) 11110–11116.
[4] J. Kaspar, P. Fornasiero, M. Graziani, Catal. Today 50 (1999) 285–298.
[5] R.J. Gorte, S. Zhao, Catal. Today 104 (2005) 18–24.
[6] S. Hilaire, X. Wang, T. Luo, R.J. Gorte, J. Wagner, Appl. Catal. A: Gen. 25 (2004) 271–276.
[7] X. Qi, M. Flytzani-Stephanopoulos, Ind. Eng. Chem. Res. 43 (2004) 3055–3062.
[8] A. Venugopal, J. Aluha, M.S. Scurrell, Catal. Lett. 90 (2003) 1–6.
[9] T. Utaka, T. Okanishi, T. Takeguchi, R. Kikuchi, K. Eguchi, Appl. Catal. A: Gen. 245 (2003) 343–351.
[10] P. Panagiotopoulou, J. Papavasiliou, G. Avgouropoulos, T. Ioannides, D.I. Kondarides, Chem. Eng. J. 134 (2007) 16–22.
[11] E.B. Fox, S. Velua, M.H. Engelhard, Y.-H. Chin, J.T. Miller, J. Kropf, C. Song, J. Catal. 260 (2008) 358–370.
[12] T. Bunluesin, R.J. GoTte, G.W. Graham, Appl. Catal. B: Environ. 15 (1998) 107–114.
[13] L. Kundakovic, M. Flytzani-Stephanopoulos, J. Catal. 179 (1998) 203–221.
[14] S.A. Hedrick, S.S.C. Chuang, A. Pant, A.G. Dastidar, Catal. Today 55 (2000) 247–257.
[15] A. Slagtern, H.M. Swaan, U. Olsbye, I.M. Dahl, C. Mirodatos, Catal. Today 46 (1998) 107–115.
[16] Y. Li, Q. Fu, M. Flytzani-Stephanopoulos, Appl. Catal. B: Environ. 27 (2000) 179–191.
[17] N.G. Valente, L.A. Arrúa, L.E. Cadús, Appl. Catal. A: Gen. 205 (2001) 201–214.
[18] S.S. Maluf, E.M. Assaf, Fuel 88 (2009) 1547–1553.
[19] A. Casanovas, C. de Leitenburg, A. Trovarelli, J. Llorcaa, Chem. Eng. J. 154 (2009) 267–273.
[20] W. Luhui, Z. Shaoxing, L. Yuan, J. Rare Earth 26 (2008) 66–70.
[21] H.-S. Roh, K.Y. Koo, W.L. Yoon, Catal. Today 146 (2009) 71–75.
[22] X. Cai, Y. Cai, W. Lin, J. Natural Gas Chem. 17 (2008) 201–207.
[23] N. Yisup, Y. Cao, W.-L. Feng, W.-L. Dai, K.-N. Fan, Catal. Lett. 99 (2005) 207–213.
[24] H.-S. Roh, H.S. Potdar, K.-W. Jun, Catal. Today 93–95 (2004) 39–44.
[25] M.C.J. Bradford, M.A. Vannice, Appl. Catal. A: Gen. 142 (1996) 97–122.
[26] N. Srisiriwat, S. Therdthianwong, A. Therdthianwong, Int. J. Hydrogen Energy 34 (2009) 2224–2234.
[27] J. Barbero, M.A. Pena, J.M. Campos-Martin, J.L.G. Fierro, P.L. Arias, Catal. Lett. 87 (2003) 211–218.
[28] S. Wang, G.Q.M. Lu, Appl. Catal. B: Environ. 16 (1998) 269–277.
[29] B. Selen, A. Erhan, Turk. J. Chem. 33 (2009) 249–256.
[30] Y. Sato, Y. Soma, T. Miyao, S. Naito, Appl. Catal. A: Gen. 304 (2006) 78–85.
[31] K.G. Azzam, I.V. Babich, K. Seshan, L. Lefferts, Appl. Catal. B: Environ. 80 (2008) 129–140.
[32] J.T. Richardson, M. Garrait, J.-K. Hung, Appl. Catal. A: Gen. 255 (2003) 69–82.
[33] T. Miyao, Y. Watanabe, M. Teramoto, S. Naito, Catal. Commun. 6 (2005) 113–117.
[34] L. Guczi, L. Takács, G. Stefler, Zs. Koppány, L. Borkó, Catal. Today 77 (2002) 237–243.
[35] H. Iida, A. Igarashi, Appl. Catal. A: Gen. 303 (2006) 192–198.
[36] E.L. Kunkes, D.A. Simonetti, J.A. Dumesic, W.D. Pyrz, L.E. Murillo, J.G. Chen, D.J. Buttrey, J. Catal. 260 (2008) 164–177.
[37] L.G.S. Pereira, V.A. Paganin, E.A. Ticianelli, Electrochim. Acta 54 (2009) 1992–1998.
[38] X. Wang, J.A. Rodriguez, J.C. Hanson, D. Gamarra, A. Martínez-Arias, M. Fernandez-Garcıia, J. Phys. Chem. B 110 (2006) 428–434.
[39] T. Tabakova, V. Idakiev, J. Papavasiliou, G. Avgouropoulos, T. Ioannides, Catal. Commun. 8 (2007) 101–106.
[40] M.G. Sanchez, J.L. Gazquez, J. Catal. 104 (1987) 120–135.
[41] E.S. Bickford, S. Velu, C. Song, Catal. Today 99 (2005) 347–357.
[42] W. Klysubun, P. Sombunchoo, N. Wongprachanukul, P. Tarawarakarn, S. Klinkhieo, J. Chaiprapa, P. Songsiriritthigul, Nucl. Instrum. Methods Phys. Res. A 582 (2007) 87–89.
[43] W. Cai, F. Wang, E. Zhan, A.C.V. Veen, C. Mirodatos, W. Shen, J. Catal. 257 (2008) 96–107.
[44] Q. Fu, W. Deng, H. Saltsburg, M. Flytzani-Stephanopoulos, Appl. Catal. B: Environ. 56 (2005) 87–95.
[45] Q. Fu, A. Weber, M. Flytzani-Stephanopoulos, Catal. Lett. 77 (2001) 87–95.
[46] V.G. Keramidas, W.B. white, J. Chem. Phys. 59 (1973) 1561–1562.
[47] J.R. McBride, K.C. Hass, B.D. Poindexter, W.H. Weber, J. Appl. Phys. 76 (1994) 2435–2441.
[48] Y. Wang, G. Xiong, X. Liu, X. Yu, L. Liu, J. Wang, Z. Feng, C. Li, J. Phys. Chem. C 112 (2008) 17265–17271.
[49] S.S. Chan, I.E. Wachs, J. Catal. 103 (1987) 224–227.
[50] R. Srnbnek, I. Hotovy, V. Malcher, A. Vincze, D. McPhail, S. Littlewood, The Third International Euro Conference on Advance Semiconductor Devices and Microsystem, Slovakia 16–18 October 2000.
[51] G.L. Markaryan, L.N. Ikryannikova, G.P. Muravieva, A.O. Turakulova, B.G. Kostyuk, E.V. Lunina, V.V. Lunin, E. Zhilinskaya, A. Aboukais, Colloids Surf. A: Physicochem. Eng. Aspects 151 (1999) 435–447.
[52] Y. Yuan, Y. Iwasawa, J. Phys. Chem. B 106 (2002) 4441–4449.
[53] M.F.L. Johnson, V.M. LeRoy, J. Catal. 35 (1974) 434–440.
[54] A.N. Webb, J. Catal. 39 (1975) 485–486.
[55] Y. Wang, Appl. Catal. B: Environ. 81 (2008) 141–149.
[56] H.-S. Roh, K.-W. Jun, W.-S. Dong, J.-S. Chang, S.-E. Park, Y.-I. Joe, J. Mol. Catal. A: Chem. 181 (2002) 137–142.
[57] Y. Zhang, Z. Li, X. Wen, Y. Liu, Chem. Eng. J. 121 (2006) 115–123.
[58] J.A. Montoya, E. Romero-Pascual, C. Gimon, P. Del Angel, A. Monzón, Catal. Today 63 (2000) 71–85.
[59] O. Thinon, F. Diehl, P. Avenier, Y. Schuurman, Catal. Today 137 (2008) 29–35.
[60] A.A. Phatak, N. Koryabkina, S. Rai, J.L. Ratta, W. Ruettinger, R.J. Farrauto, G.E. Blau, W.N. Delgass, F.H. Ribeiro, Catal. Today 123 (2007) 224–234.
[61] Y. Iwasawa (Ed.), X-ray Absorption Fine Structure for Catalysts and Surfaces, World Scientific Publishing, Singapore, 1995, p. p60.
[62] J. Zhang, X. Ju, Z.Y. Wu, T. Liu, T.D. Hu, Y.N. Xie, Chem. Mater. 13 (2001) 4192–4197.
[63] A.M. Shahin, F. Grandjean, G.J. Long, T.P. Schuman, Chem. Mater. 17 (2005) 315–321.
[64] P. Nachimuthu, W.C. Shih, R.S. Liu, L.Y. Jang, J.M. Chen, J. Solid State Chem. 149 (2000) 408–413.
[65] T. Ressler, J. Wienold, R.E. Jentoft, T. Neisius, J. Catal. 210 (2002) 67–83.
[66] F. Hilbrig, C. Michel, G.L. Haller, J. Phys. Chem. 96 (24) (1992) 9893–9899.
[67] S. Hilaire, X. Wang, T. Luo, R.J. Gorte, J. Wagner, Appl. Catal. A: Gen. 215 (2001) 271–278.
[68] G. Jacobs, E. Chenu, P.M. Patterson, L. Williams, D. Sparks, G. Thomas, B.H. Davis, Appl. Catal. A: Gen. 258 (2004) 203–214.